Journal of Materials Chemistry C

What is the role of planarity and torsional freedom for aggregation in a π-conjugated donor-acceptor model oligomer?

Journal:	*Journal of Materials Chemistry C*
Manuscript ID	TC-ART-01-2020-000217.R1
Article Type:	Paper
Date Submitted by the Author:	28-Feb-2020
Complete List of Authors:	Wedler, Stefan; Bayreuth University, Soft Matter Optoelectronics, Experimentalphysik II Bourdick, Axel; Bayreuth University, Biofluid Simulation and Modeling, Theoretische Physik VI Athanasopoulos, Stavros; Universidad Carlos III de Madrid, Departamento de Física; Universidad Carlos III de Madrid Gekle, Stephan; Bayreuth University, Biofluid Simulation and Modeling, Theoretische Physik VI Panzer, Dr. Fabian; Universitat Bayreuth, Experimental Physics II McDowell, Caitlin; University of California Santa Barbara Nguyen, Thuc-Quyen; UCSB, Chemistry and Biochemistry Bazan, Guillermo; National University of Singapore Köhler, Anna; Bayreuth University, Soft Matter Optoelectronics, Experimentalphysik II; University of Bayreuth, BIMF and BPI

What is the role of planarity and torsional freedom for aggregation in a π-conjugated donor-acceptor model oligomer? †

Stefan Wedler[1], Axel Bourdick[2], Stavros Athanasopoulos[3], Stephan Gekle[2], Fabian Panzer[1], Caitlin McDowell[4], Thuc-Quyen Nguyen[4], Guillermo C. Bazan[5], Anna Köhler[1,6*]

[1] Soft Matter Optoelectronics, Experimentalphysik II, University of Bayreuth, Bayreuth 95440, Germany.

[2]Biofluid Simulation and Modeling, Theoretische Physik VI, Universität Bayreuth, Bayreuth 95440, Germany

[3]Departamento de Física, Universidad Carlos III de Madrid, Avenida Universidad 30, 28911 Leganés, Madrid, Spain.

[4]Center for Polymers and Organic Solids, Departments of Chemistry & Biochemistry and Materials, University of California, Santa Barbara

[5]Departments of Chemistry and Chemical Engineering, National University of Singapore, Singapore, 119077

[6]Bayreuth Institute of Macromolecular Research (BIMF) and Bavarian Polymer Institute (BPI), University of Bayreuth, 95440 Bayreuth, Germany.

*e-mail: Anna.Koehler@uni-bayreuth.de

†Electronic supplementary information (ESI) available.

Abstract

Ordered domains play a central role in determining the properties of organic semiconductors, and thereby the performance of their devices. The molecules in these ordered domains are often characterized by planar backbone conformations. We investigate the influence of backbone planarity on the propensity to form ordered structures using a pair of model oligomers with electron poor benzothiadiazole moieties and electron rich thiophene units. The two oligomers differ by their central unit, where a bithiophene unit either allows for flexible twists ("TT"), or where it is bridged as a cyclopentadithiophene to provide a rigid planar connection ("CT"). Temperature dependent absorption and luminescence spectroscopy in solution along with atomistic simulations show that the more flexible TT readily forms aggregates upon cooling, while CT instead first forms non-emissive excimers and only forms aggregates below 200K. Molecular dynamics simulations reveal that aggregation in TT can only be accounted for if TT takes on a planar conformation in the course of the aggregation process. The stronger intermolecular interaction in TT compared to the banana-shaped CT can then be related to the larger number of attractive intermolecular interactions between the various subunits. Thus, molecular flexibility is an important design parameter, as it determines the accessibility of ordered intermolecular structures and ultimately device performance.

1. Introduction

The performance of organic semiconductor devices such as organic solar cells (OSCs), transistors (OFETs) and light emitting diodes (OLEDs) depends not just on the chemical structure of the π-conjugated oligomers used. Rather, over the last decade we learned that the molecular self-assembly, and the resulting intermolecular interactions, as well as disorder can be decisive in controlling device performance.[1-7] An attractive feature of organic semiconductors is that they can be processed from solution, provided they are appropriately substituted,[8-11] so that fabrication avenues such as printing or roll-to-roll processing are possible.[12-17]

To understand the complex film formation processes that are involved in the fabrication of devices from solution, we need to first understand the interactions that prevail between chromophores in solution. A suitable means to examine the formation of structures with short-range or even long-range order, referred to as "aggregates", is to cool down a solution.[18] This approach keeps the concentration constant while the solvent quality gradually deteriorates. When such studies are carried out on π-conjugated polymers or oligomers, one finds the appearance of emission or absorption due to aggregates is preceded by a planarization process of the polymer or oligomer.[19-23] Also, structural design to enhance the planarization of a polymer backbone by inserting heteroatoms with interactions that lead to conformational locks has been demonstrated to successfully increase the propensity to form ordered structures.[24-27] For oligomers such as acenes or coronenes, it is well known that an extended planar π-system is conducive to aggregation.[28-31] In fact, the challenge is frequently to suppress excessive aggregation by insertion of suitable sidechains or sterically demanding groups.[32-36] From these studies one may infer that a rigidified planar backbone is a guiding principal to obtain compounds that can self-assemble into ordered structures.

However, there are reports that indicate that the aggregation process itself is inducing the planar conformation of the chromophore. For example, De Leneer et al. studied how aggregates form for the polymer MEH-PPV.[37] In their quantum chemical studies, they found that the timescale for conformational fluctuations, notably rotations of the vinyl and phenyl units, are slowed down when two chain segments are brought close. This allows for the build-up of attractive interactions and the eventual formation of a planar, aggregated segment. Further, Kärnbratt et al. investigated the self-assembly process of linear porphyrin oligomers. From the very sudden onset of aggregation they conclude that a planar backbone structure has been induced by the assembly process, rather than vice versa.[29] In these cases one would expect that the molecules need to possess a certain degree of flexibility to eventually access the conformation required for ordered structures.

Here we address the question whether pre-existing backbone planarity is of advantage for the self-assembly process, or whether the required planarity may instead also be induced during the assembly process by considering two model oligomers referred to as “TT” and “CT”. Figure 1 shows the chemical structures of these molecules. They differ only in their central unit. For TT, the central unit is a flexible bithiophene, marked in red. The hexyl sidechains induce a dihedral angle of 68°, as obtained from DFT calculations, while the flexibility is preserved. In particular, TT is able to planarize. The stiff molecule CT comprises a cyclopentadithiophene, marked in blue, forcing it to be planar. These model oligomers are very similar to compounds used in efficient solar cells, such as T1,[38-41] which are frequently made in a D-A-D-A-D type structure with electron-rich (D) and electron-poor (A) subunits.[31, 42, 43]

This paper is structured as follows. After introducing the methods in section 2, we describe in section 3 our observations and interpretation of the spectroscopic measurements taken in solution. In section 4, these results are compared to and discussed against the predictions made by molecular dynamics simulations. Time dependent density functional theory (TD-DFT) calculations on the excited state structure in dimers are discussed in section 5. Section 6 finally reports and discusses the observation of emission from cis- and trans-conformations of TT. A concluding summary is provided in section 7.

2. Methods

Sample preparation

The molecules 7,7'-(3,3'-dihexyl-[2,2'-bithiophene]-5,5'-diyl)bis(6-fluoro-4-(5-hexylthiophen-2-yl)benzo[c][1,2,5]thiadiazole) (**TT**) and 7,7'-(4,4-dihexyl-4H-cyclopenta[2,1-b:3,4-b']dithiophene-2,6-diyl)bis(6-fluoro-4-(5-hexylthiophen-2-yl)benzo[c][1,2,5]thiadiazole) (**CT**) were synthesized as reported previously,[44] their structures are shown in Figure 1. Solutions with different concentrations were prepared inside a glovebox using O_2-free anhydrous hexane from Acros. To ensure complete dissolution, the solutions were heated to 50 °C and stirred up to one hour. We used quartz glass cuvettes with a thickness of 1.00 mm (10.00 mm) for solutions with concentrations of $5.0 \cdot 10^{-5}$ M and higher ($5.0 \cdot 10^{-6}$ M and lower) for optical characterization.

Emission and absorption measurements

Temperature dependent absorption and emission spectra were measured with a home-built setup.[23] Detection was performed utilizing a CCD camera (Andor iDus 420) coupled to an Andor Shamrock 303 spectrograph. For excitation we used a 405nm diode laser from Coherent for all CT

measurements and a 485 nm diode laser from PicoQuant for all TT measurements, both operating in continuous wave mode. Emission spectra were corrected for the efficiencies of all optical components as well as for changes of the absorbance at the laser wavelength. All samples were put into a temperature controlled continuous-flow cryostat (Oxford Instruments) using liquid helium as the coolant. A waiting time of 15 minutes before measurement was sufficient after reaching each temperature to ensure thermal equilibration of the sample.

Time-correlated single photon counting measurements were performed using a FluoTime 200 spectrometer from PicoQuant and a 485 nm diode laser operating in pulsed mode for excitation. Signal acquisition was performed utilizing the counting module PicoHarp 300E (PicoQuant).

Quantum-Chemical Calculations

Ground state optimizations of the individual molecules with the side chains were performed at the density functional theory (DFT) level using the ωB97XD long-range corrected exchange-correlation functional[45] and a split valence 6-31G** polarized double zeta basis set. We have used a range separation parameter of ω=0.13 au^{-1} that has been previously obtained by tuning the fundamental gap of the TT molecule.[44] This functional provides comparable performance to coupled cluster CCSD(T) calculations in substituted bithiophenes.[46] Excited state geometry optimizations and vertical transition energies of the individual molecules and the dimers were obtained with linear response time dependent density functional theory (TD-DFT). All DFT and TD-DFT calculations were carried out with Gaussian 09 software.[47] Calculated absorption spectra for the single molecules as well as aggregated dimers can be found in the ESI (Section 1) and show excellent agreement with experimental data.

To quantify the extent of intermolecular exciton delocalization on the CT and TT dimers we have computed the participation ratio of the dominant hole and electron natural transition orbitals (NTOs),[7] defined as:

$$PR = (\rho_{mol1}^2 + \rho_{mol2}^2)^{-1}$$

with $\rho_{moli} = \sum_{j \in moli}^{N} C_j^2$

C_j are the corresponding coefficients of the normalised NTOs. PR takes values between 1 and 2: when PR = 1 the natural transition orbital is fully localized on a single molecule while when PR = 2 it is equally delocalized between the two molecules. To obtain information on the intermolecular charge transfer character we define a CTC parameter as:

$$CTC = \left|\frac{\Delta h - \Delta e}{2}\right|$$

where

$$\Delta h = \sum_{j \in mol1}^{N} C_{j,HOMO}^2 - \sum_{j \in mol2}^{N} C_{j,HOMO}^2$$

$$\Delta e = \sum_{j \in mol1}^{N} C_{j,LUMO}^2 - \sum_{j \in mol2}^{N} C_{j,LUMO}^2$$

The CTC parameter takes values between 0 and 1: CTC = 0 indicates an excitation without intermolecular charge transfer character and CTC = 1 indicates an excitation with complete charge transfer character, meaning the hole (HOMO) NTO is completely localized over the first molecule and the electron (LUMO) NTO is completely localized over the opposite molecule.

MD-Simulations

We performed molecular dynamics simulation with Gromacs[48-51] using the Gromos 54a7 force field.[52] The structure files were generated with JME.[53] The force field files for CT[54] and TT[55] were generated with the automated force field topology builder and repository.[56-58]

In order to make the simulations more accurate we calculated the charge distribution and the potential energy surface (PES) of the dihedral angle between the various donor and acceptor parts of the molecules and between the two thiophene rings in the central donor unit of TT with DFT and adjusted our MD models to reproduce the behaviour calculated with DFT. Structure and topology files for the solvent hexane were taken from the ATB database.[59] More details about how the models were built are specified in the ESI, Section 2. For the simulations all-atom force field topologies were used. We used a cubic box of two solute molecules and between 500 and 1100 solvent molecules. We defined the reaction coordinate as the distance between the center of mass of the central donor unit of TT and the center of mass of the middle ring of the central donor unit of CT. Starting configurations for the umbrella windows were generated from a random configuration from which we squeezed the solute molecules together and pulled them apart along the reaction coordinate. Configuration snapshots were saved in steps of 0.04 nm. Each simulation was equilibrated and conducted as NPT ensemble. To cover the whole configurational phase space, we sampled the reaction pathways independently eight times for TT and eleven times for CT with hexyl sidechains. For the free energy graphs with CH_3 sidechains we sampled the reaction pathway of TT and CT four times each. The free energy graphs are averaged over all these runs. The simulation time varied from 60 ns to 800 ns per window. The free energy graphs were calculated with umbrella sampling[60] and

the *Weighted Histogram Analysis Method*,[61] which is implemented in Gromacs as *gmx wham*. Two-dimensional free energy surfaces were calculated with well-tempered metadynamics,[62-65] which was carried out using the open-source community-developed PLUMED library version 2.2 integrated as a plugin to the Gromacs software.[66, 67] Visualisation was done with VMD.[68] All Simulations were performed at T = 300 K. Further details about the simulation parameters and the used force constants can also be found in the ESI, Section 2.

3. Optical spectroscopy

Results

We study the influence of torsional rigidity on the aggregation behaviour using the two molecules shown in Figure 1. They consist of typical building blocks for donor-acceptor-type molecules used in organic solar cells and differ only in their central unit, which consists of connected thiophenes ("CT") or twisted thiophenes ("TT"). The stiff molecule, thereafter referred to as CT, comprises a cyclopentadithiophene marked in blue. For the molecule called TT, the central unit is a flexible bithiophene, marked in red. Its alkyl sidechains result in a twisted geometry with a dihedral angle of 68° as determined by quantum chemical calculations (see section 6) and in agreement with literature.[44]

We conducted temperature dependent absorption and emission measurements in hexane between 300 K and 180 K to investigate their aggregation properties in solution and compare three different concentrations. Figure 2 shows the absorption and emission of TT in hexane at $5.0 \cdot 10^{-6}$ M, $5.0 \cdot 10^{-5}$ M and $2.5 \cdot 10^{-4}$ M. All emission spectra are normalized to coincide at the high energy side at about 2.1 eV. For the lowest concentration of $5.0 \cdot 10^{-6}$ M, both absorption and emission only change little upon cooling. The unstructured absorption (Figure 2b) increases in intensity and the peak position shifts from 2.53 eV at 300 K to 2.47 eV at 200 K. In emission (Figure 2a) we also observe a redshift of the peak around 2.0 eV by 20 meV and a reduction of the linewidth upon cooling. Furthermore, an additional high-energy shoulder at 2.15 eV emerges upon cooling. We discuss the origin of this shoulder further below in section 6.

For the intermediate concentration of $5.0 \cdot 10^{-5}$ M (Figure 2c,d) we again observe a redshift and increase in absorption until 230 K (solid yellow line) upon cooling. At 220 K and below, new spectral features emerge at lower energies both in absorption and emission. A structured absorption feature with the first peak at 1.95 eV and further vibronic replicas at 2.12 eV and 2.30 eV is observed. Concomitantly, the unstructured absorption band centered at 2.5 eV disappears, resulting in an

isosbestic point at 2.35 eV. The additional luminescence feature shows peaks at 1.81 eV and 1.64 eV, and a shoulder at 1.46 eV. Again, the high-energy shoulder at 2.15 eV emerges upon cooling.

The spectral changes upon cooling become more drastic when we increase the concentration further to $2.5 \cdot 10^{-4}$ M (Figure 2e,f). The absorption band reduces in intensity below 260 K. The emerging absorption feature shows a strong raising baseline and the structure is smeared out. This is characteristic for light scattering from small particles. Similarly, in emission, the peaks at 1.81 eV and 1.64 eV grow in from 260 K onwards and keep increasing. This is accompanied by a change in relative weight of the vibrational peaks, so that the peak at 1.64 eV eventually dominates and the overall shape is reminiscent of a classical excimer-type emission (except for being more structured).[30] In addition to this evolution at the red side of the spectrum, the already mentioned shoulder at 2.15 eV emerges at low temperatures, independent of concentration.

The changes of the more rigid CT with temperature and concentration are displayed in Figure 3. The emission spectra are normalized to coincide at the low energy side around 1.7 eV. For the lowest concentration (Figure 3a,b), both absorption and emission change little upon cooling. Overall, the intensity of the absorption increases slightly, the spectra shift to the red by 40 meV and the linewidth (full width at half maximum) of the absorption narrows by 29 meV. A Franck-Condon analysis reveals that the apparent change of the peak ratios is due to the decreasing linewidth, as detailed in the ESI, Section 3.

When increasing the concentration to $5.0 \cdot 10^{-5}$ M (Figure 3c,d), we notice a decrease in absorption intensity for the spectra taken at 200 K, 190 K and 180 K. This is accompanied by a reduction in the ratio between the 0-0 peak at about 2.03 eV and the 0-1 peak at about 2.18 eV as well as a broadening of the low energy tail. The emission spectra have a similar shape at lower concentration. However, the relative contribution of the 0-0 peak at 1.9 eV is less pronounced and at the lowest temperature (180 K) we observe an additional weak feature below 1.6 eV.

In absorption, at the highest concentration (Figure 3f), there is a reduction of the 0-0 peak at about 2.05 eV from 280 K onwards compared to the 0-0 peak intensity observed for the lower concentrations (for better comparison among different concentrations see ESI, Section 4). The overall absorption intensity reduces from 240 K onwards, and the spectra exhibit a low energy shoulder at 1.85 eV for 200 K and below, as well as a scattering offset. In emission (Figure 3e) the trends already observed for the intermediate concentration are more pronounced. In particular, we observe a clear low energy feature with peaks at 1.55 eV and 1.40 eV for 200 K and below.

We displayed the emission spectra in Figures 2 and 3 in a normalized manner to allow for a good comparison of the spectral shapes. The relative emission intensities, integrated over the entire

spectrum and normalized to unity at room temperature, are displayed in Figure 4a and b. For TT, the overall intensity remains constant until the lower energy band appears (at 230 K and 260 K for the intermediate and higher concentration, respectively), and then reduces steeply. For CT, the emission intensity reduces for the intermediate and higher concentration from about 250 K onwards, which does not correlate in an obvious way with spectral changes.

More information on the low energy bands can be obtained from their spectral shapes. For the concentration of 2.5×10^{-4} M, we separated the low energy band in TT (CT) spectrally from the high energy band. For this, we took the emission spectrum at 260 K (210 K) that displays only the high energy feature, normalized it to the high energy side of the spectra taken at lower temperatures, and subtracted it. The resulting difference spectrum consists only of the low energy band and is shown in Figure 4c. With decreasing temperature, there is a reduction of the 0-0 peak at 1.8 eV for the low energy band in TT. The energy of the 0-0 peak stays constant during the transition, in contrast to an ongoing bathochromic shift observed for aggregate emission in several polymers like P3HT or PCPDTBT.[19, 20] For CT, the separated spectra of the low energy band below 210 K are identical within experimental uncertainty and we only present the result for 180 K, which also shows a reduced intensity of the 0-0 peak.

Discussion

Cooling down a solution is a well-known means to reduce the quality of a solvent to promote aggregation phenomena while keeping the overall concentration unchanged. The different spectral evolutions we observe for CT and TT seem to suggest that the nature of the connecting unit has a strong impact on their propensity to aggregate.

The evolution of the spectra for TT is comparatively straightforward to interpret, as it follows the pattern observed for other conjugated polymers or molecules such as P3HT.[18, 19, 69] Consider for example the absorption at the intermediate concentration, 5×10^{-5} M. The bathochromic shift and increase in oscillator strength in absorption implies that the conjugation length in the molecule increases upon cooling, suggesting a freezing out of torsional motion between the various heterocyclic units and stronger planarization of the backbone. Changes in the refractive index and/or polarizability of the solvent upon cooling have minor impact on the spectral positions (see ESI, Section 5.[70] The appearance of the isosbestic point below a critical temperature T_c of 230 K indicates the transition from individually solvated molecules into aggregates, and this is accompanied by the appearance of associated emission features. At higher concentrations, this transition sets in at higher temperatures. We attribute the appearance of an apparent long low energy tail in the absorption at the highest concentration to light-scattering due to a larger size of the aggregated conglomerates.

The reduction in emission intensity upon aggregate formation, the reduction of the 0-0 peak upon cooling (Figure 4a and c), and the increase of the non-radiative decay rate from 0.3 ns^{-1} at 300 K to 1.2 ns^{-1} at 180 K are characteristic for a predominantly H-type interaction (see ESI, Section 6).[71] Thus, we can conclude that TT forms weakly interacting H-type aggregates when reducing the solvent quality by cooling.

In contrast, the evolution of the CT spectra is more complex. The small redshift upon cooling in the absorption of the dilute solution indicates a freezing out of torsional modes in the vicinity of the benzothiadiazole that increases the overall conjugation length, which is less pronounced in emission, consistent with a typically already more planar geometry of the excited state.[72] Despite the more planar, rigid character, signs of aggregate formation are less pronounced than for TT. Clear signatures in absorption and emission for the formation of a weakly interacting aggregate prevail in the higher concentrated solution, i.e. at $2.5x10^{-4}$ M, only below 210 K, and for the intermediate concentration below 200 K. There are, however, more subtle spectral changes already below 240 K, notably in the ratios of the 0-0 to 0-1 absorption peaks. It is striking that there is a clear decrease in overall emission intensity below 250 K for the intermediate and higher concentrations, even though this is not accompanied by any emissive features. This suggests that, below 250 K, CT first forms some non-emissive species, and emissive aggregates are only formed at higher concentrations and lower temperatures. A similar observation has been made earlier for the aggregation process in pyrene-derivatives.[73]

This is an unexpected result for CT. For the polymers and oligomers we investigated so far, including TT reported here, we always observed that a planarization of the backbone preceded the formation of aggregates, and that these aggregates had sufficient oscillator strength so that they could be identified in absorption and emission. Moreover, increasing the backbone planarity through conformational locks has previously been demonstrated to enhance the tendency to form ordered, even crystalline structures.[24, 74] In contrast, here, it seems that the rigid nature of the connection does not assist the formation of aggregates, but rather induces the formation of non-emissive excimer-like species.

4. Molecular Dynamics simulations

Results

In previous work we found that reduced torsional motion precedes aggregation,[18] and an initial planarization prior to aggregation is also what we observed here for CT and TT, as discussed in

section 3. It is thus not immediately clear why CT shows less signs of aggregation than TT. A possible explanation could be that the sidechains of the central CT unit might prevent approximation of adjacent molecules as these chains are pointing out of the molecular plane, whereas the sidechains lie in the molecular plane for TT. To test this hypothesis, we conducted molecular dynamics (MD) simulations for the molecules with the full hexyl sidechains, as well as for the molecules where the central sidechains are replaced by CH_3. Different rotamers, meaning different orientations of the benzothiadiazole unit, were sampled in the simulations, as their existence was observed for related compounds.[75, 76] We found no significant difference among the possible rotamers in our simulations. The key observable of the simulations is the free energy of the system, which consists of two single molecules surrounded by 500 to 1100 solvent molecules. Free energy curves are computed using Umbrella Sampling as detailed in the Method Section and the ESI, Section 2.

Figure 5 compares the resulting average free energies as a function of intermolecular distance, defined as the center of mass distance for the central units, alongside with corresponding dimer geometries. These schematics serve to illustrate the mean configurations of snapshots in the MD simulation at the different minima along the free energy curves. We find that upon approximation the free energy of two molecules decreases. For both, TT and CT, this pathway involves several minima. For TT, we find that the two molecules approach predominantly by successively sliding over each other along the long axis of the molecule. Due to the central twist, the two wings do not lie parallel on top of each other, but rather twist around each other (Figure 5b, position 4, and movie clip deposited as ESI). When the sidechains are replaced by CH_3 groups, it seems that this process becomes facilitated, resulting in a significantly deeper minimum at closest approximation.

For CT, we also observe predominantly a sliding process along the long axis. Due to the rigid central cyclopentadithiophene, CT has a banana shape. Correspondingly, there are two possible conformations, depending on the relative orientation of the central cyclopentadithiophene group (Figure 5d, position 3, and movie clips deposited as ESI). The two molecules may arrange with their curvature in opposite direction (type A) or in the same direction (type B). For type A, the sidechains on the two central units are also orientated opposite, thus not causing any steric effects. For type B, the final geometry contains an offset by one ring unit along the molecular long axis, thus avoiding direct interaction of the sidechains. The prevalence of *two* possible energetically favourable arrangements in CT as opposed to only one in TT is further supported by metadynamics calculations, as evident from Figure 5e as well as Figures S2.6 and S2.7 in the ESI.

Replacing the hexyl side chains by CH_3 hardly affects this arrangement. As a result, there is very little increase in free energy gain when the long alkyl sidechains are replaced by CH_3. Importantly, we do not observe a significantly lower minimum of the free energy for CT without sidechains as compared

to TT without sidechains. Thus, the sidechains do not seem to be the decisive factor that renders TT more prone to aggregation than CT.

From the free energy curves obtained for the molecules with sidechains, we would, in fact, expect a stronger propensity to aggregation from CT, at variance with experiment. However, in the MD calculation of Figure 5a we considered a twisted dihedral potential in TT, which was derived from DFT calculations of a single molecule. In other words, the calculations did not take into account any possible planarization effects that may result from a change of the electronic structure caused by intermolecular interactions upon approximation. In fact, TT was found to planarize in the solid state[44, 77] while planarization has also been observed in substituted oligothiophenes.[78, 79] Therefore, it is conceivable that the molecule also planarizes when two of them approach in order to form an aggregate in solution, and this may need to be considered in the MD calculation. Thus we calculated the free energy between two TT molecules when the rotational potential of central bithiophene has a minimum for both sulphurs of the molecule pointing into the same direction ("cis") or opposite direction ("trans"). The result is shown in Figure 6. Allowing for a planarization of TT indeed results in significant energy gain upon aggregation. Compared to the conformation with a twisted central bithiophene, the cis conformation is favoured by 3.5 k_BT, and the trans-conformation is stabilized by 5.0 k_BT. Importantly, for both planar conformations the free energy is lower for TT as compared to CT. The same conclusion still applies when the sidechains are replaced by CH_3, as discussed in the ESI (Section 7).

Allowing for a planarized central bithiophene unit thus results in a free energy curve that is consistent with the experimental observations of a higher critical temperature as well as clear aggregate signatures for TT. We also found that lack of steric hindrance by sidechains is not the reason for the strong tendency to aggregate that we see experimentally for TT. To understand in more detail what promotes the aggregation, we thus proceed to consider interactions between adjacent units in our model dimers. For TT, the final average configuration obtained by MD is illustrated as inset in Figure 6. In the trans-configuration, the molecules adopt a slight zig-zag shape and they arrange offset by one unit along the long molecular axis. As a result, five rings lie directly opposite each other. This comprises four pairs where an electron-rich thiophene is opposite an electron-poor benzothiadiazole, and one thiophene-thiophene pair. In contrast, for CT, there are less points of contact. For type A (Figure 5), only two benzothiadiazole rings lie opposite each other. For type B, there is slightly more interaction, that is, two thiophene-benzothiadiazole pairs form and the central bithiophene-benzothiadiazole units lie adjacent such as to be able to interact. The interactions between these subunits is attractive, in particular for donor-acceptor type pairs, as already shown earlier[41] and detailed further in the ESI (Section 8). Thus, it appears that the stronger

interaction in the TT dimer can be rationalized by its zig-zag like geometry that allows for more contact points where attractive interactions can take place.

Discussion

To summarize the insight gained from the MD simulations, we found that planarization of the TT molecule is essential to reproduce its strong propensity to form aggregates. We can therefore say that a more planar structure, preferably trans-planar, is needed to promote aggregation. This planar configuration may form in-situ after an initial pairing of twisted molecules, i.e. through the sliding mechanism in Figure 5b. There is evidence that a temporarily more planar structure can itself be induced by the proximity of two molecules. For example, De Leener et al. performed a combination of molecular dynamics and quantum chemistry calculations for the polymer MEH-PPV.[37] They could show that conformational fluctuations are large for isolated molecules on short timescales. However, these fluctuations happen on longer timescales in the bulk, making polymer chains more planar on average once they are surrounded by other chains. It is conceivable that a similar mechanism contributes here to render the TT molecule more planar when a second molecule comes close, in addition to the electronic-structure-induced planarization discussed above. This would result in the planarity required to allow for persistent aggregation.

The amount of interaction between two adjacent molecules depends on the number of units that come close, and thus it depends on its shape. The MD calculations indicate that the slight zig-zag geometry of TT leads to more contact points than the banana shape of CT, and this seems to advance the propensity for aggregation. At first sight, this seems to be at variance with the results by Welch et al. [80] for related banana-shaped oligomers. They reported that a stronger bend angle is favourable for crystallization, while according to our results, a weaker bend angle inducing more contact points should seem advantageous. The resolution to this apparent contradiction lies in the overall symmetry of the arrangement. The banana-shaped oligomers addressed by Welch et al. arrange in a type A conformation. Here, attractive interactions can result from the contacts between acceptor units. However, the central unit does not contribute to this at a close distance. Rather, there is an unfavourable need to repel solvent molecules between the central units, and the interaction between the central units is itself repulsive (see ESI, Section 8).[41] A stronger bend angle here indeed alleviates this constraint while still preserving the acceptor interactions. The situation is different for the zig-zag geometry of TT, where the attractive interactions between the four donor-acceptor pairs dominate, or for type B of CT where the central units are also attractive.

5. Quantum chemical calculations

Having established what causes the stronger propensity of TT to aggregate, we reconsider the spectral signatures of both molecules. For TT, additional features appear simultaneously upon cooling in the absorption and the emission spectra, consistent with our interpretation of an H-type aggregate. The continuous reduction of the 0-0 peak with cooling in the aggregate emission (compare Figure 4c) can be understood as a sign of increasing strength of electronic interaction, as observed earlier for instance in P3HT or PCPDTBT.[19, 20] In contrast, for CT, signs of aggregation emerged in the absorption spectra only below 200 K (Figure 3). The emission from the aggregate has a broad shape with a 0-0 peak that is slightly lower than the 0-1 peak, indicative of some H-like electronic interaction (Figure 4). However, the emission intensity in CT reduces already from 250 K onwards, even though no additional features appear in absorption or emission. The reduction of emission intensity suggests that an additional non-radiative decay channel opens up. We already mentioned that the most likely candidate for this is the formation of a non-emissive excimer. Such species that form as a precursor to aggregates have been reported before by Haedler et al. for pyrene-derivatives.[73] The formation of more weakly bound precursor species such as excimers would be consistent with the lower number of attractive contact points formed for CT. We have conducted time dependent density functional theory (TD-DFT) calculations to consider the electronic nature of possible dimers formed for TT and CT.

For this, we averaged the dimer structures from the MD simulations, focusing on the relevant conformations with minimal intermolecular distance. For TT we used only the trans-planar aggregate, while for CT we considered both, type A and type B conformers separately. Based on these, we have prepared dimers with one of the molecules on the ground state geometry and the other molecule on the first excited state geometry. These conformations served as starting points for TD-DFT geometry optimizations of the first excited state of the dimer without imposing any symmetry constraints. We thus monitor the structural relaxation of the dimer upon photoexcitation and internal conversion of one of the molecules and therefore the propensity of the aggregate to form excimer states.

Table 1 shows the optimized geometries for all three dimers and the corresponding electron-hole pair natural transition orbitals. The relaxed excited state geometry for the TT dimer has a plane-to-plane distance of 3.66 Å, which is close to the ground state plane-to-plane distance of 3.63 Å. The natural transition orbitals delocalize over the whole dimer, yielding a small charge transfer character of 0.23, and the oscillator strength is low. This is consistent with experiment, as the emission intensity decreases significantly upon aggregation.

The picture is different for CT. Upon excitation, the dimer geometry relaxes such that the plane-to-plane distance decreases significantly. This is most pronounced for the type A conformation where the plane-to-plane distance reduces by 0.20 Å. The excitation is delocalized equally over both molecules of the dimer. Emission from this excited state has no charge transfer character, yet also no oscillator strength. The significant geometry change upon excitation, lack of charge transfer character and lack of oscillator strength imply that this is quasi a textbook example for a non-emissive excimer.[81] Moreover, it is also at lower energy than the type B conformation. For the type B dimer, we find a reduction in plane-to-plane distance still by 0.12 Å. The transition has a large charge transfer character, where the electron is localized mainly on one molecule and the hole is equally delocalized over both molecules of the dimer. The transition to the ground state has a finite oscillator strength. Between 250 K and 200 K we have not observed any emission feature that could be assigned to emission from type B dimers. Evidently, energy is funnelled to a type A excimer-like precursor, which accounts for the reduction in emission intensity, until emissive aggregates can form below 200 K.

6. High energy peak in TT

As a final point we consider briefly the emission feature observed in TT at 2.15 eV for all temperatures and all concentrations, even when diluting further to $5.0 \cdot 10^{-7}$ M (see ESI, Section 9). The fact that this shoulder is independent of concentration excludes intermolecular origins for this spectral feature. We note that this feature does not allow for a description of the overall emission spectra in terms of a single Franck-Condon-transition (see ESI, Section 10). However, assuming two very similar progressions at different energies gives a satisfactory description of the spectral shape. This is shown in Figure 7a exemplary for the 200 K emission spectrum. For both progression, we used a Gaussian linewidth of σ=59 meV and the same 3 vibrational energies at 55 meV, 135 meV and 180 meV as observed in the Raman spectra, that we tentatively associated with librations or rotations, C-H in plane bending modes on the rings and C=C stretching modes, respectively.[81] A detailed description of the fitting procedure and parameters is given in the ESI (Section 10). To identify the origin of the two features, we performed time-correlated single photon counting measurements at two energies at 200 K. Figure 7b shows the decay curves at 2.23 eV and at 1.89 eV as well as the instrument response function. Both features show about the same exponential decay of τ=2.2±0.2 ns from about 1 ns onward. At shorter times, the signal at 2.23 eV is dominated by different contributions from the instrument response function. More precisely, Raman scattering of the 2850 cm^{-1} mode from the solvent takes place and contributes at very short times.[82] The same decay time at both energies excludes a transition from a possible higher energy state into a lower

energy state. Rather, both features seem to pertain to very similar excited states. Dual emission from two states on the same chromophore such as S_1 and S_2 can be safely excluded as origin since the two features differ by only 150 meV. After excitation into a S_2 state, internal conversion into S_1 would be very fast and outcompete radiative decay due to the energy gap law (Kasha's rule). Furthermore, identical emission spectra upon different excitation energies (3.06 eV and 2.56 eV) as well as DFT calculations safely exclude different rotamers as the origin of the high energy feature.

A further possibility is to consider that both conformations can be accessed after excitation. Figure 7c shows the potential energy surface for TT as a function of the dihedral angle between the two central thiophenes for the ground state (GS) and lowest excited state (ES) before and after relaxation subsequent to a transition. The S_0 to S_1 transition (absorption) occurs vertically from the $GS_{relaxed}$ curve to the ES_{GS} curve. In the relaxed GS, the conformation has a cis-like character. After the vertical transition, the molecule relaxes into the $ES_{relaxed}$ curve. In this process, it can relax to the cis-like minimum in the $ES_{relaxed}$ curve at 50° or to the trans-like minimum above 140°, from where they can decay to the GS_{ES} curve with a slightly larger (cis-like) or smaller (trans-like) transition energy. Keeping in mind the limitations of DFT calculations for quantitative values for donor-acceptor type compounds, and recalling the case of polyacetylene,[83] we can still safely associate the cis-like configuration with the higher energy transition and the trans-like configuration with the lower energy transition. Thus, the high-energy shoulder we observe in TT is attributed to emission from molecules where a cis-like configuration of the central bithiophene still prevails.

When wondering why there is no energy transfer to molecules in the trans-like configuration it is worth recalling that the minimum in the GS geometry is for the cis-like configuration, and the trans-like configuration is mostly accessed through the excited state. This explains why emission from both configurations can be observed.

7. Conclusions

In this study we address the role of backbone torsion and planarity in the formation of ordered structures using a pair of model oligomers with a twisted central bithiophene unit (TT) or a rigid central cyclopentadithiophene (CT). Unexpectedly, the more flexible TT is found more disposed to form weakly emissive H-type aggregates than planar CT. It turns out that the propensity of these oligomers to form ordered structures is not controlled by steric demands of their sidechains. Rather, it can be rationalized by considering the number of attractive interactions that can take place between the various subunits along the oligomer. A certain flexibility of the backbone assists in establishing these intermolecular contact points. In the MD calculations we find that the

experimentally observed aggregation in TT can only be explained when TT is allowed to adopt planar conformation. In this case, the more zig-zag like backbone conformation of TT leads to a larger number of attractive interactions than the banana-shape of CT. This larger interaction accounts not only for the stronger tendency of TT to aggregate, but also can elucidate why TT directly forms emissive aggregates while CT, upon cooling, first forms non-emissive excimer-type precursors until aggregate formation sets in below 200 K.

Acknowledgements

We acknowledge financial support by the Bavarian State Ministry of Science, Research, and the Arts (StMWK) through the Collaborative Research Network "Solar Technologies go Hybrid" and through the Bavarian Center "BaCaTec". S.W. was supported by the Elite Network Bavaria (ENB) in the framework of the Elite Study Program "Macromolecular Science" and "MINT Lehramt plus". A.B. was supported by the German Science Foundation (GRK1640 "Photophysics of Synthetic and Biological Multichromophoric Systems"). We acknowledge support through the computational resources provided by the Bavarian Polymer Institute and the Jülich Supercomputing Center. S.G. thanks the Volkswagen Foundation. This work was also supported by the Universidad Carlos III de Madrid, the European Union's Seventh Framework Programme for research, technological development and demonstration under grant agreement No. 600371, el Ministerio de Economía, Industria y Competitividad (COFUND2014-51509), el Ministerio de Educación, cultura y Deporte (CEI-15-17), Banco Santander and el Ministerio de Ciencia, Innovación y Universidades (RTI2018-101020-B-I00).

Conflicts of interest

There are no conflicts of interest to declare.

Literature

1. D. Moseguí González, C. J. Schaffer, S. Pröller, J. Schlipf, L. Song, S. Bernstorff, E. M. Herzig and P. Müller-Buschbaum, *ACS Appl. Mater. Interfaces*, 2017, **9**, 3282-3287.
2. F.-J. Kahle, C. Saller, S. Olthof, C. Li, J. Lebert, S. Weiß, E. M. Herzig, S. Hüttner, K. Meerholz, P. Strohriegl and A. Köhler, *J. Phys. Chem. C*, 2018, **122**, 21792-21802.
3. G. Feng, J. Li, Y. He, W. Zheng, J. Wang, C. Li, Z. Tang, A. Osvet, N. Li, C. J. Brabec, Y. Yi, H. Yan and W. Li, *Joule*, 2019, **3**, 1765-1781.
4. N. Gasparini, S. Kahmann, M. Salvador, J. D. Perea, A. Sperlich, A. Baumann, N. Li, S. Rechberger, E. Spiecker, V. Dyakonov, G. Portale, M. A. Loi, C. J. Brabec and T. Ameri, *Adv. Energy Mater.*, 2019, **9**, 1803394.
5. Y.-s. Huang, S. Westenhoff, I. Avilov, P. Sreearunothai, J. M. Hodgkiss, C. Deleener, R. H. Friend and D. Beljonne, *Nat. Mater.*, 2008, **7**, 483-489.
6. T. A. Papadopoulos, L. Muccioli, S. Athanasopoulos, A. B. Walker, C. Zannoni and D. Beljonne, *Chem. Sci.*, 2011, **2**, 1025-1032.
7. A. Sharma, S. Athanasopoulos, P. C. Tapping, R. P. Sabatini, O. F. McRae, M. Müllner, T. W. Kee and G. Lakhwani, *J. Phys. Chem. C*, 2018, **122**, 23910-23916.
8. Y. Lin, Y. Li and X. Zhan, *Chem. Soc. Rev.*, 2012, **41**, 4245-4272.
9. Y. Chen, X. Wan and G. Long, *Acc. Chem. Res.*, 2013, **46**, 2645-2655.
10. A. a. F. Eftaiha, J.-P. Sun, I. G. Hill and G. C. Welch, *Journal of Materials Chemistry A*, 2013, **2**, 1201-1213.
11. S. D. Collins, N. A. Ran, M. C. Heiber and T.-Q. Nguyen, *Adv. Energy Mater.*, 2017, **7**, 1602242.
12. F. C. Krebs, S. A. Gevorgyan and J. Alstrup, *J. Mater. Chem.*, 2009, **19**, 5442-5451.
13. F. C. Krebs, T. Tromholt and M. Jørgensen, *Nanoscale*, 2010, **2**, 873-886.
14. R. Søndergaard, M. Hösel, D. Angmo, T. T. Larsen-Olsen and F. C. Krebs, *Mater. Today*, 2012, **15**, 36-49.
15. B. Qu and S. R. Forrest, *Appl. Phys. Lett.*, 2018, **113**, 053302.
16. J. Yang, Y. Lin, W. Zheng, A. Liu, W. Cai, X. Yu, F. Zhang, Q. Liang, H. Wu, D. Qin and L. Hou, *ACS Appl. Mater. Interfaces*, 2018, **10**, 22485-22494.
17. K. S. Wienhold, V. Körstgens, S. Grott, X. Jiang, M. Schwartzkopf, S. V. Roth and P. Müller-Buschbaum, *ACS Appl. Mater. Interfaces*, 2019, **11**, 42313-42321.
18. F. Panzer, H. Bässler and A. Köhler, *J. Phys. Chem. Lett.*, 2017, **8**, 114-125.
19. F. Panzer, M. Sommer, H. Bässler, M. Thelakkat and A. Köhler, *Macromolecules*, 2015, **48**, 1543-1553.
20. C. Scharsich, F. S. U. Fischer, K. Wilma, R. Hildner, S. Ludwigs and A. Köhler, *J. Polym. Sci., Part B: Polym. Phys.*, 2015, **53**, 1416-1430.
21. D. Raithel, S. Baderschneider, T. B. de Queiroz, R. Lohwasser, J. Köhler, M. Thelakkat, S. Kümmel and R. Hildner, *Macromolecules*, 2016, **49**, 9553-9560.
22. M. Reichenberger, J. A. Love, A. Rudnick, S. Bagnich, F. Panzer, A. Stradomska, G. C. Bazan, T.-Q. Nguyen and A. Köhler, *J. Chem. Phys.*, 2016, **144**, 074904.
23. M. Reichenberger, D. Kroh, G. M. M. Matrone, K. Schötz, S. Pröller, O. Filonik, M. E. Thordardottir, E. M. Herzig, H. Bässler, N. Stingelin and A. Köhler, *J. Polym. Sci., Part B: Polym. Phys.*, 2018, **56**, 532-542.
24. H. Huang, L. Yang, A. Facchetti and T. J. Marks, *Chem. Rev.*, 2017, **117**, 10291-10318.
25. N. E. Jackson, B. M. Savoie, K. L. Kohlstedt, M. Olvera de la Cruz, G. C. Schatz, L. X. Chen and M. A. Ratner, *J. Am. Chem. Soc.*, 2013, **135**, 10475-10483.
26. K. J. Thorley and I. McCulloch, *J. Mater. Chem. C*, 2018, **6**, 12413-12421.
27. W. Zhang, Z. Mao, N. Zheng, J. Zou, L. Wang, C. Wei, J. Huang, D. Gao and G. Yu, *J. Mater. Chem. C*, 2016, **4**, 9266-9275.
28. M. Levitus, K. Schmieder, H. Ricks, K. D. Shimizu, U. H. F. Bunz and M. A. Garcia-Garibay, *J. Am. Chem. Soc.*, 2001, **123**, 4259-4265.

29. J. Kärnbratt, M. Gilbert, J. K. Sprafke, H. L. Anderson and B. Albinsson, *J. Phys. Chem. C*, 2012, **116**, 19630-19635.
30. J. Gierschner and S. Y. Park, *J. Mater. Chem. C*, 2013, **1**, 5818.
31. A. Mishra and P. Bäuerle, *Angew. Chem. Int. Ed.*, 2012, **51**, 2020-2067.
32. Q. Yan, Y. Zhou, Y.-Q. Zheng, J. Pei and D. Zhao, *Chem. Sci.*, 2013, **4**, 4389.
33. Y. Liu, C. Mu, K. Jiang, J. Zhao, Y. Li, L. Zhang, Z. Li, J. Y. L. Lai, H. Hu, T. Ma, R. Hu, D. Yu, X. Huang, B. Z. Tang and H. Yan, *Adv. Mater.*, 2015, **27**, 1015-1020.
34. W. Chen, X. Yang, G. Long, X. Wan, Y. Chen and Q. Zhang, *J. Mater. Chem. C*, 2015, **3**, 4698-4705.
35. W. Chen and Q. Zhang, *J. Mater. Chem. C*, 2017, **5**, 1275-1302.
36. C. B. Nielsen, S. Holliday, H.-Y. Chen, S. J. Cryer and I. McCulloch, *Acc. Chem. Res.*, 2015, **48**, 2803-2812.
37. C. De Leener, E. Hennebicq, J.-C. Sancho-Garcia and D. Beljonne, *J. Phys. Chem. B*, 2009, **113**, 1311-1322.
38. Y. Sun, G. C. Welch, W. L. Leong, C. J. Takacs, G. C. Bazan and A. J. Heeger, *Nat. Mater.*, 2012, **11**, 44-48.
39. J. A. Love, C. M. Proctor, J. Liu, C. J. Takacs, A. Sharenko, T. S. v. d. Poll, A. J. Heeger, G. C. Bazan and T.-Q. Nguyen, *Adv. Funct. Mater.*, 2013, **23**, 5019-5026.
40. J. A. Love, I. Nagao, Y. Huang, M. Kuik, V. Gupta, C. J. Takacs, J. E. Coughlin, L. Qi, T. S. van der Poll, E. J. Kramer, A. J. Heeger, T.-Q. Nguyen and G. C. Bazan, *J. Am. Chem. Soc.*, 2014, **136**, 3597-3606.
41. A. Bourdick, M. Reichenberger, A. Stradomska, G. C. Bazan, T.-Q. Nguyen, A. Köhler and S. Gekle, *J. Phys. Chem. B*, 2018, **122**, 9191-9201.
42. J. E. Coughlin, A. Zhugayevych, I. Bakus, Ronald C., T. S. van der Poll, G. C. Welch, S. J. Teat, G. C. Bazan and S. Tretiak, *J. Phys. Chem. C*, 2014, **118**, 15610-15623.
43. G. C. Welch, L. A. Perez, C. V. Hoven, Y. Zhang, X.-D. Dang, A. Sharenko, M. F. Toney, E. J. Kramer, T.-Q. Nguyen and G. C. Bazan, *J. Mater. Chem.*, 2011, **21**, 12700.
44. C. Zhou, Q. Cui, C. McDowell, M. Seifrid, X. Chen, J.-L. Brédas, M. Wang, F. Huang and G. C. Bazan, *Angew. Chem.*, 2017, **129**, 9446-9449.
45. J.-D. Chai and M. Head-Gordon, *J. Chem. Phys.*, 2008, **128**, 084106.
46. T.-J. Lin and S.-T. Lin, *PCCP*, 2015, **17**, 4127-4136.
47. M. J. Frisch, G. W. Trucks, H. B. Schlegel, G. E. Scuseria, M. A. Robb, J. R. Cheeseman, G. Scalmani, V. Barone, G. A. Petersson, H. Nakatsuji, X. Li, M. Caricato, A. V. Marenich, J. Bloino, B. G. Janesko, R. Gomperts, B. Mennucci, H. P. Hratchian, J. V. Ortiz, A. F. Izmaylov, J. L. Sonnenberg, Williams, F. Ding, F. Lipparini, F. Egidi, J. Goings, B. Peng, A. Petrone, T. Henderson, D. Ranasinghe, V. G. Zakrzewski, J. Gao, N. Rega, G. Zheng, W. Liang, M. Hada, M. Ehara, K. Toyota, R. Fukuda, J. Hasegawa, M. Ishida, T. Nakajima, Y. Honda, O. Kitao, H. Nakai, T. Vreven, K. Throssell, J. A. Montgomery Jr., J. E. Peralta, F. Ogliaro, M. J. Bearpark, J. J. Heyd, E. N. Brothers, K. N. Kudin, V. N. Staroverov, T. A. Keith, R. Kobayashi, J. Normand, K. Raghavachari, A. P. Rendell, J. C. Burant, S. S. Iyengar, J. Tomasi, M. Cossi, J. M. Millam, M. Klene, C. Adamo, R. Cammi, J. W. Ochterski, R. L. Martin, K. Morokuma, O. Farkas, J. B. Foresman and D. J. Fox, Gaussian 09 Rev. E.01, Gaussian, Inc., Wallingford, CT, 2013
48. S. Pronk, S. Páll, R. Schulz, P. Larsson, P. Bjelkmar, R. Apostolov, M. R. Shirts, J. C. Smith, P. M. Kasson, D. van der Spoel, B. Hess and E. Lindahl, *Bioinformatics*, 2013, **29**, 845-854.
49. M. J. Abraham, T. Murtola, R. Schulz, S. Páll, J. C. Smith, B. Hess and E. Lindahl, *SoftwareX*, 2015, **1-2**, 19-25.
50. S. Páll, M. J. Abraham, C. Kutzner, B. Hess and E. Lindahl, in *Solving Software Challenges for Exascale*, eds. S. Markidis and E. Laure, Springer International Publishing, 2015, pp. 3-27.
51. B. Hess, C. Kutzner, D. van der Spoel and E. Lindahl, *J. Chem. Theory Comput.*, 2008, **4**, 435-447.
52. N. Schmid, A. P. Eichenberger, A. Choutko, S. Riniker, M. Winger, A. E. Mark and W. F. van Gunsteren, *Eur. Biophys. J.*, 2011, **40**, 843.
53. P. Ertl, *J. Cheminformatics*, 2010, **2**, 1.

54. ATB Database: CT Structure and Toplogy Files, https://atb.uq.edu.au/molecule.py?molid=285451, (accessed June 2019).
55. ATB Database: TT Structure and Toplogy Files, https://atb.uq.edu.au/molecule.py?molid=285450, (accessed June 2019).
56. A. K. Malde, L. Zuo, M. Breeze, M. Stroet, D. Poger, P. C. Nair, C. Oostenbrink and A. E. Mark, *J. Chem. Theory Comput.*, 2011, **7**, 4026-4037.
57. S. Canzar, M. El-Kebir, R. Pool, K. Elbassioni, A. K. Malde, A. E. Mark, D. P. Geerke, L. Stougie and G. W. Klau, *J. Comput. Biol.*, 2013, **20**, 188-198.
58. K. B. Koziara, M. Stroet, A. K. Malde and A. E. Mark, *J. Comput. Aided Mol. Des.*, 2014, **28**, 221-233.
59. ATB Database: Hexane Structure and Toplogy Files, https://atb.uq.edu.au/molecule.py?molid=467, (accessed June 2019).
60. J. Kästner, *WIREs Comput. Mol. Sci.*, 2011, **1**, 932-942.
61. J. S. Hub, B. L. de Groot and D. van der Spoel, *J. Chem. Theory Comput.*, 2010, **6**, 3713-3720.
62. A. Barducci, G. Bussi and M. Parrinello, *Phys. Rev. Lett.*, 2008, **100**, 020603.
63. B. M. Dickson, *Phys. Rev. E*, 2011, **84**, 037701.
64. A. Laio and M. Parrinello, *Proc. Natl. Acad. Sci.*, 2002, **99**, 12562-12566.
65. A. Barducci, M. Bonomi and M. Parrinello, *WIREs Comput. Mol. Sci.*, 2011, **1**, 826-843.
66. G. A. Tribello, M. Bonomi, D. Branduardi, C. Camilloni and G. Bussi, *Comput. Phys. Commun.*, 2014, **185**, 604-613.
67. The PLUMED consortium, *Nat. Methods*, 2019, **16**, 670-673.
68. W. Humphrey, A. Dalke and K. Schulten, *J. Mol. Grapics*, 1996, **14**, 33-38.
69. A. Köhler, S. T. Hoffmann and H. Bässler, *J. Am. Chem. Soc.*, 2012, **134**, 11594-11601.
70. J. Gierschner, H.-G. Mack, L. Lüer and D. Oelkrug, *The Journal of Chemical Physics*, 2002, **116**, 8596.
71. N. J. Hestand and F. C. Spano, *Chem. Rev.*, 2018, **118**, 7069-7163.
72. D. Raithel, L. Simine, S. Pickel, K. Schötz, F. Panzer, S. Baderschneider, D. Schiefer, R. Lohwasser, J. Köhler, M. Thelakkat, M. Sommer, A. Köhler, P. J. Rossky and R. Hildner, *Proc. Natl. Acad. Sci.*, 2018, **115**, 2699-2704.
73. A. T. Haedler, H. Misslitz, C. Buehlmeyer, R. Q. Albuquerque, A. Köhler and H.-W. Schmidt, *ChemPhysChem*, 2013, **14**, 1818-1829.
74. H. Hu, P. C. Y. Chow, G. Zhang, T. Ma, J. Liu, G. Yang and H. Yan, *Acc. Chem. Res.*, 2017, **50**, 2519-2528.
75. C. McDowell, K. Narayanaswamy, B. Yadagiri, T. Gayathri, M. Seifrid, R. Datt, Sean M. Ryno, M. C. Heifner, V. Gupta, C. Risko, S. P. Singh and G. C. Bazan, *Journal of Materials Chemistry A*, 2018, **6**, 383-394.
76. J. Shi, A. Isakova, A. Abudulimu, M. v. d. Berg, O. K. Kwon, A. J. Meixner, S. Y. Park, D. Zhang, J. Gierschner and L. Lüer, *Energy & Environmental Science*, 2018, **11**, 211-220.
77. M. T. Seifrid, G. N. M. Reddy, C. Zhou, B. F. Chmelka and G. C. Bazan, *J. Am. Chem. Soc.*, 2019, **141**, 5078-5082.
78. G. Barbarella, M. Zambianchi, A. Bongini and L. Antolini, *Adv. Mater.*, 1992, **4**, 282-285.
79. G. Macchi, B. M. Medina, M. Zambianchi, R. Tubino, J. Cornil, G. Barbarella, J. Gierschner and F. Meinardi, *PCCP*, 2009, **11**, 984-990.
80. G. C. Welch, I. Bakus, Ronald C., S. J. Teat and G. C. Bazan, *J. Am. Chem. Soc.*, 2013, **135**, 2298-2305.
81. A. Köhler and H. Bässler, *Electronic Processes in Organic Semiconductors: An Introduction*, Wiley-VCH Verlag GmbH & Co. KGaA, Weinheim, Germany, 2015.
82. F. F. Cleveland and P. Porcelli, *J. Chem. Phys.*, 1950, **18**, 1459-1461.
83. H. Eckhardt, *J. Chem. Phys.*, 1983, **79**, 2085-2086.

Figures and Tables

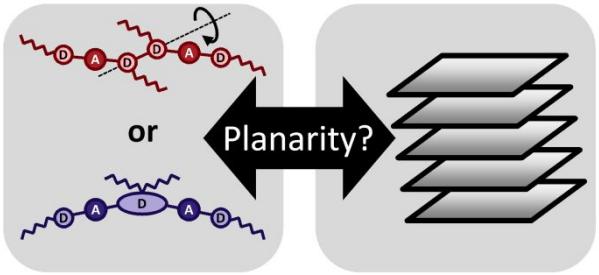

Table of contents figure

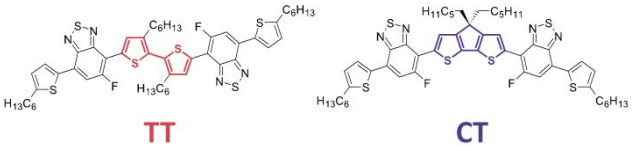

Figure 1:

Chemical structures of TT and CT.

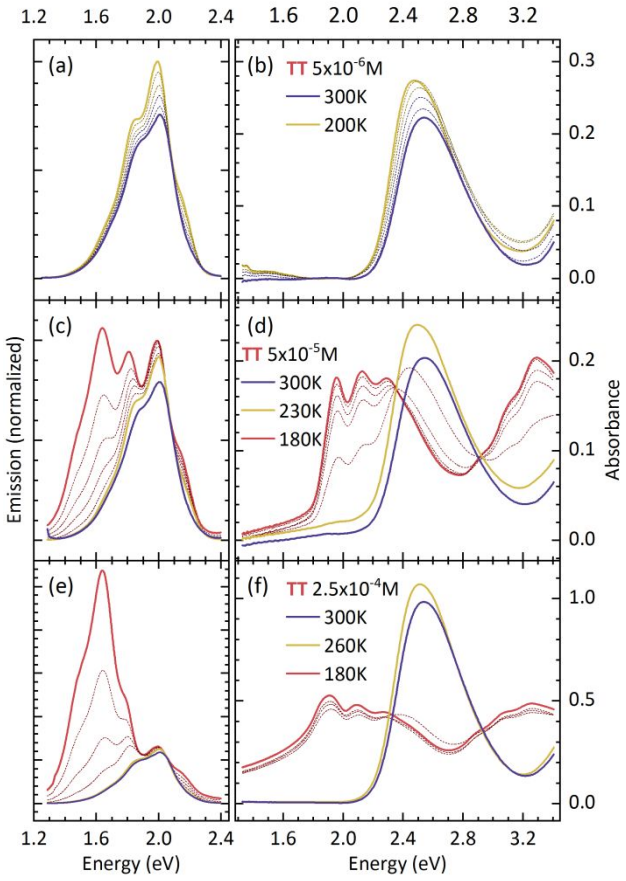

Figure 2:

Absorption (b,d,f) and emission (a,c,e) spectra of TT in hexane for different temperatures at a concentration of (a,b) $5.0 \cdot 10^{-6}$ M, (c,d) $5.0 \cdot 10^{-5}$ M and (e,f) $2.5 \cdot 10^{-4}$ M. Emission spectra are normalized to about 2.08 eV. Spectra taken at characteristic temperatures are drawn with solid lines and given in the legend. Temperatures in between are shown in steps of 20 K for a), b) and between 180 K and 260 K in e) and f), and in steps of 10 K between 180 K and 230 K for c) and d).

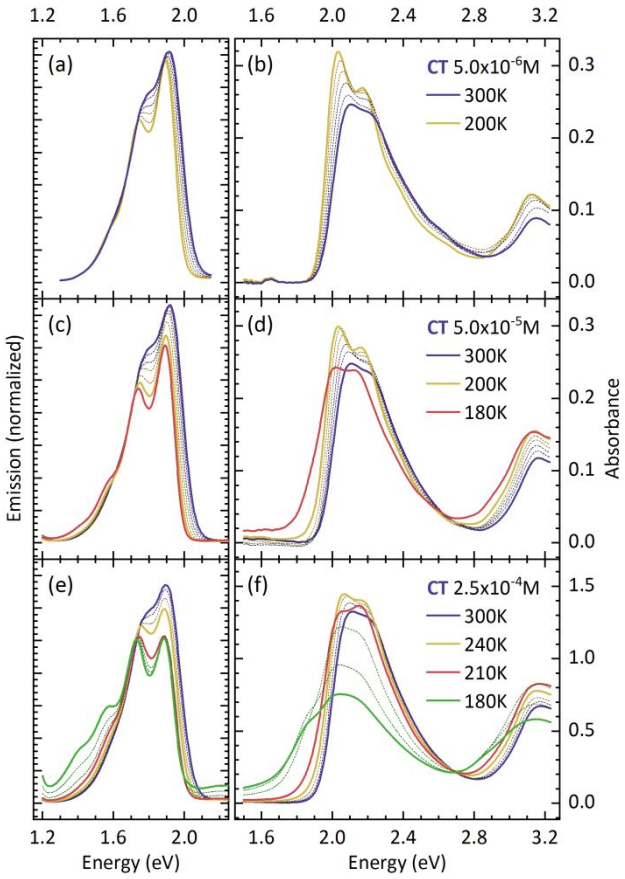

Figure 3:

Absorption (b,d,f) and emission (a,c,e) spectra of CT in hexane for different temperatures at a concentration of (a,b) $5.0 \cdot 10^{-6}$ M, (c,d) $5.0 \cdot 10^{-5}$ M and (e,f) $2.5 \cdot 10^{-4}$ M. Emission spectra are normalized to about 1.7 eV. Spectra taken at characteristic temperatures are drawn with solid lines and given in the legend. Temperatures in between are shown in steps of 20 K for a), b), c), d) and between 240 K and 300 K in e) and f), and in steps of 10 K between 180 K and 210 K for e) and f).

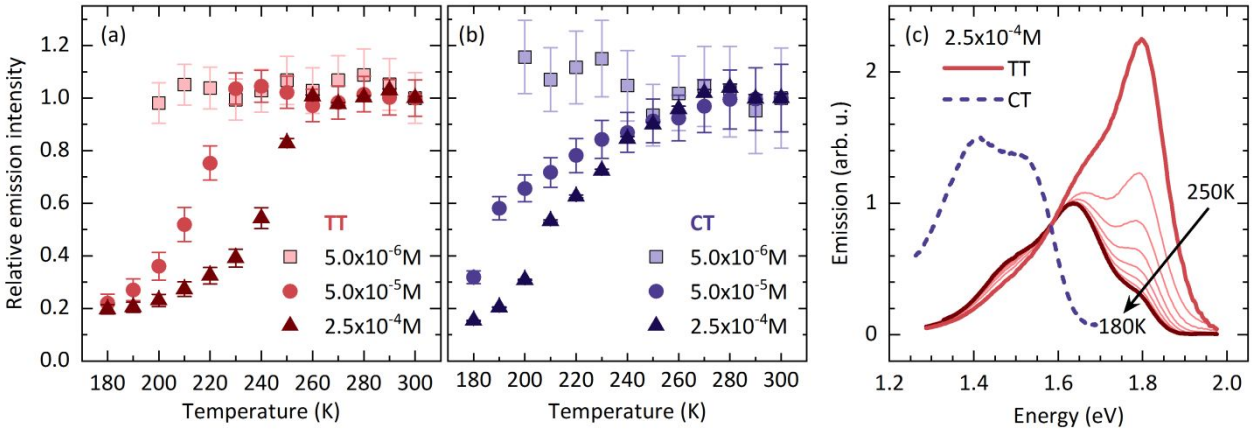

Figure 4:

Relative emission intensity as function of temperature for different concentrations for (a) TT and (b) CT. (c) Separated aggregate emission spectra at the concentration of $2.5 \cdot 10^{-4}$ M. The spectra for TT are normalized to 1.6 eV and are taken in steps of 10 K as indicated by the arrow. For CT only the spectrum at 180 K is shown.

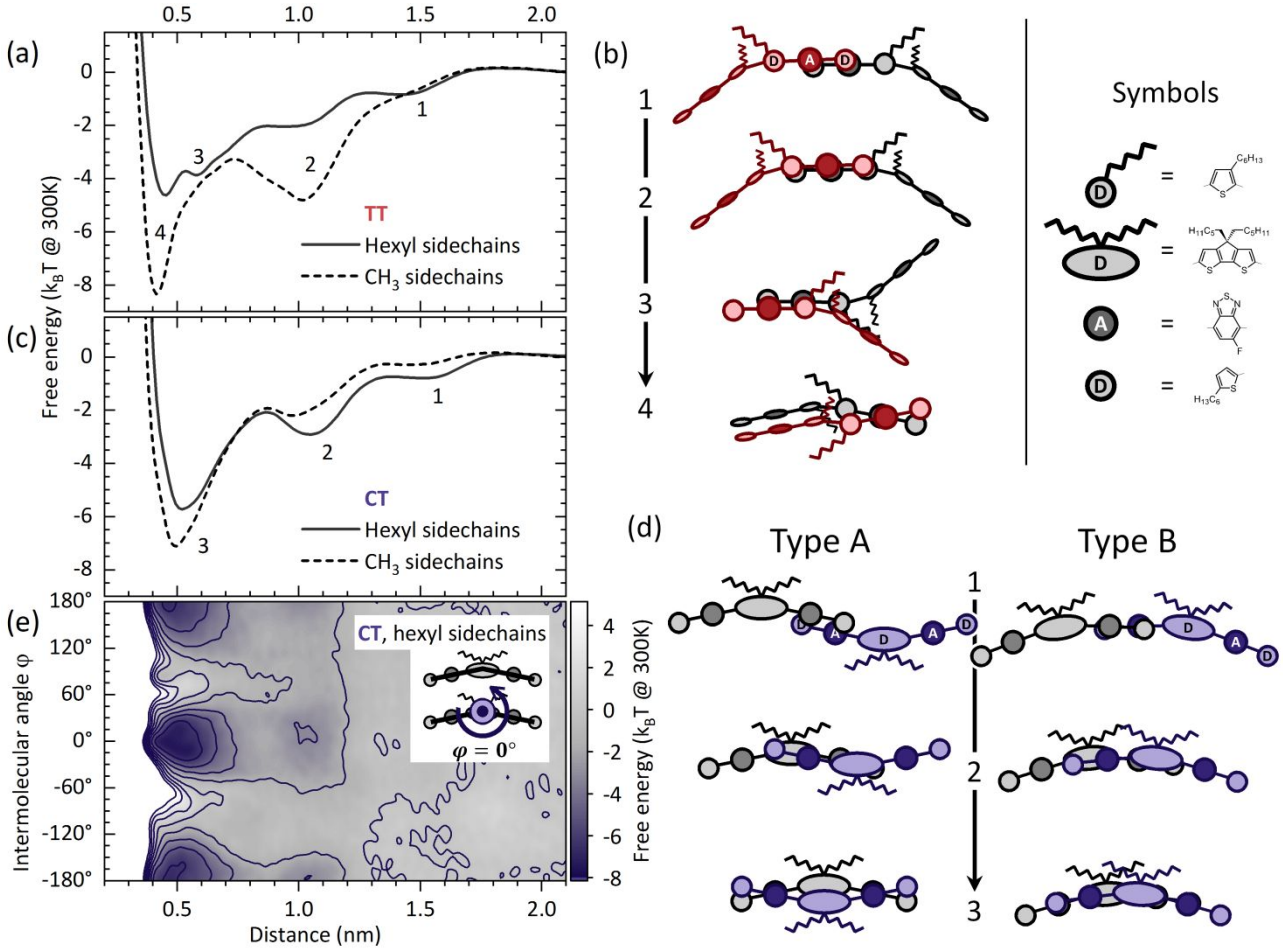

Figure 5

(a) Free energy curves for the TT dimer with hexyl and CH_3 sidechains as function of the distance of the central bithiophenes. (b) Dimer geometries for the closest distance and along the free energy curve as indicated in (a). (c) Free energy curves for the CT dimer with hexyl and CH_3 sidechains as function of the distance of the central cyclopentadithiophenes. (d) Dimer geometries for the closest distance and along the free energy curve as indicated in (c). For CT there are two final conformations possible. (e) Two-dimensional free energy surface calculated by metadynamics for the CT dimer with hexyl side chains as function of intermolecular distance and intermolecular angle φ. The inset visualizes φ and shows the conformation for φ = 0.

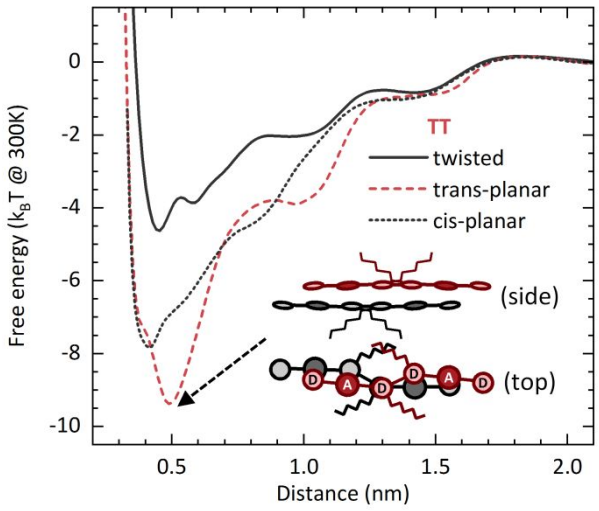

Figure 6

Free energy simulations of TT for the twisted conformation and both planar conformations. The sketch shows the intermolecular geometry for the trans-planar dimer with highest energetic stabilisation.

Table 1

TD-DFT results for the optimized S1 state of each dimer for TT in the trans-planar conformation and CT type A and type B. We display visualizations of the dominant electron-hole pair natural transition orbitals, the corresponding transition energy, the oscillator strength (f), the charge transfer character (CTC), and the plane-to-plane distances for ground state and excited state.

	TT (trans)	CT (Type A)	CT (Type B)
Electron	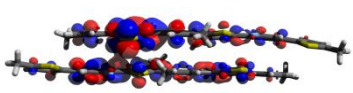	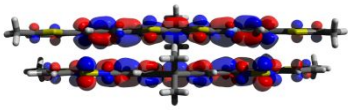	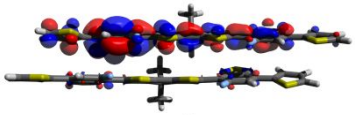
Hole	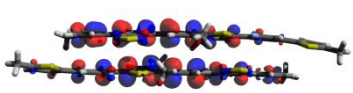	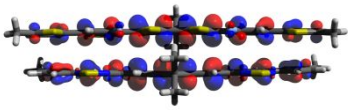	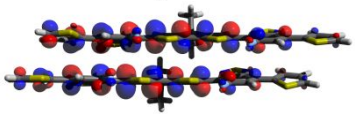
Energy (eV)	1.69	1.56	1.68
f	0.0014	0.0000	0.21
CTC	0.23	0.00	0.39
Plane-to-plane distance (Å)			
Ground state	3.63	3.68	3.64
Excited state	3.66	3.48	3.52
Difference	+0.02	-0.20	-0.12

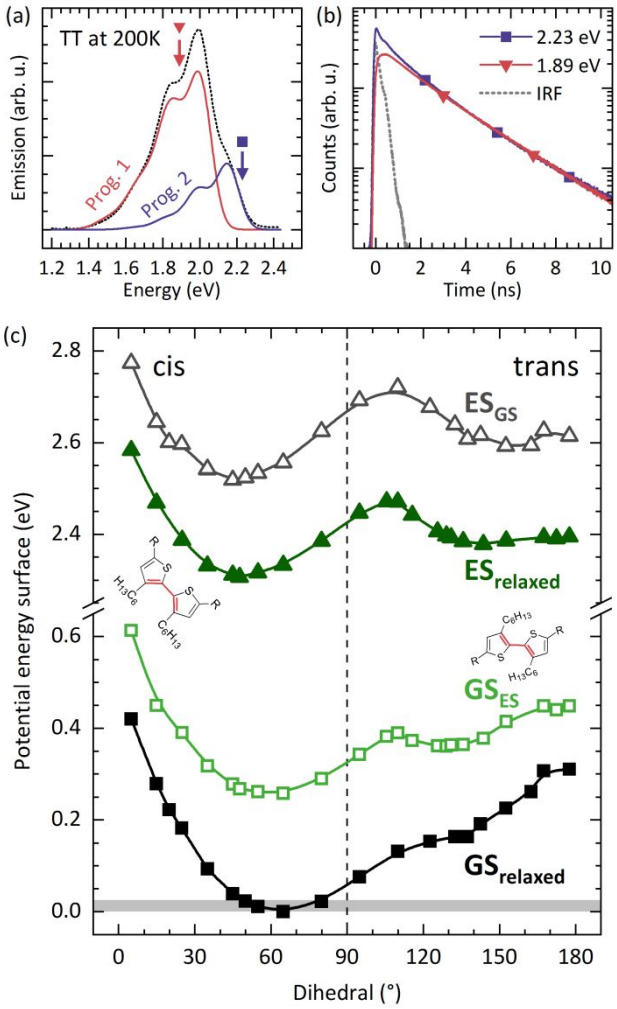

Figure 7

(a) Decomposition of the TT emission spectrum at 200 K into a low energy progression (progression 1) and a high energy progression (progression 2). The symbols mark the spectral positions of the decay curves. (b) Decay curves at 200 K monitored at the energies marked in (a). The grey broken line shows the instrumental response measured at the excitation energy. (c) Potential energy surface of the central thiophene-thiophene dihedral angle in TT for ground state (GS) and excited state (ES) obtained by DFT and TD-DFT. The calculations are performed in the relaxed geometries (filled symbols) and in the non-relaxed geometries after electronic transition (open symbols). The grey area indicates k_BT at room temperature. The dashed line serves to separate the cis-like conformations visually from the trans-like configurations.

TOC entry

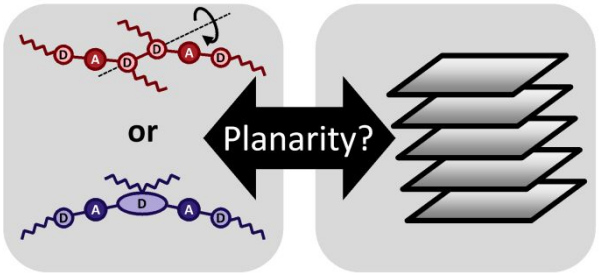

We compare the aggregation properties of two model compounds, differing in their stiffness, in solution by a combined spectroscopic and computational approach.